



Numerical simulation of fume formation process in GMA welding

Shinichi Tashiro¹ · Anthony B. Murphy² · Manabu Tanaka¹

Received: 20 March 2018 / Accepted: 14 September 2018 / Published online: 25 September 2018
© International Institute of Welding 2018

Abstract

In order to clarify fume formation process in GMA welding, quantitative investigation based on understanding of interaction *between* the electrode, the arc, and the weld pool is indispensable. This study aims to clarify the fume formation process theoretically through numerical analysis. A fume formation model consisting of a homogeneous nucleation model, a heterogeneous condensation model, and a coagulation model was coupled with a GMA welding model. A series of processes such as evaporation of metal vapor from molten metal, transport of the metal vapor in the arc, fume formation from the metal vapor, and transport of the fume to the surrounding was investigated by employing this coupled simulation model. In this paper, the influence on the fume formation process of changing the shielding gas from Ar to CO₂ and the associated change in arc characteristics, leading to different droplet formation and metal transfer phenomena, is discussed. As a result, it was clarified that the fume particles produced around the droplet were transported into the arc to be evaporated again and a large number of fine fume particles were produced in the downstream region of the plasma flow near the base metal in Ar GMA welding. In contrast, approximately 30% of all fume particles produced around the droplet were transported directly to the surrounding and the other particles were transported into the arc to be evaporated to produce fume particles in the downstream region in CO₂ arc welding.

Keywords Fume · GMA welding · Argon · CO₂ · Metal transfer · Numerical simulation

1 Introduction

In arc welding, high-temperature metal vapor is generated by evaporation of molten metal; depending on the type of arc welding, this can include the molten tip of the welding wire, the droplets, and the weld pool [1, 2]. The metal vapor is cooled rapidly as it diffuses to the fringes of the arc. Metal nanoparticles, with sizes in the range 1–100 nm, are formed through nucleation from the metal vapor and grow through condensation of metal vapor; we call these the primary particles. Some of these particles collide and produce secondary particles, with sizes up to over 1 μm. The particles have the

appearance of smoke, which ascends from the arc and is known as welding fume.

Inhalation of welding fume is a significant occupational health problem. The size of the fume particles gives them a high probability of deposition in parts of the lungs where rapid clearance mechanisms are not effective. Further, certain metals, such as chromium (particularly hexavalent chromium) and nickel, are of particular concern when inhaled [3].

Most papers on welding fume are concerned with the chemical composition and generation rate of the fume for consumable electrode welding methods, such as gas metal arc (GMA) and shielded metal arc (SMA) welding, because of their widespread use in manufacturing industries. For example, Kobayashi et al. observed fume generation in SMA welding by employing a high-speed video camera. It was qualitatively explained that metal vapor was produced in the lower part of the arc column and generated fume due to rapid cooling, together with condensation and oxidation. They also showed that the amount of metal vapor produced from the droplet was greater than that from the weld pool [4]. Jenkins et al. measured the chemical composition of fume in SMA and GMA welding by energy-dispersive spectroscopy (EDS) [5]. Bosworth and Deam discussed the influence of droplet size on

Recommended for publication by Study Group 212 - The Physics of Welding

✉ Shinichi Tashiro
tashiro@jwri.osaka-u.ac.jp

¹ Joining and Welding Research Institute, Osaka University, 11-1 Mihogaoka, Osaka, Ibaraki 576-0047, Japan

² CSIRO Manufacturing, PO Box 218, Lindfield, NSW 2070, Australia

the fume generation rate in GMA welding [6]. Until quite recently, the research on welding fume was almost exclusively confined to experimental observations, sometimes combined with engineering calculations (e.g., [7]).

There has been little theoretical research directed towards clarifying the mechanism of fume formation; this requires a quantitative investigation, taking into account of the interactions between the electrode, the arc, and the weld pool. In the cases of GMA and SMA welding, this is a particularly complex problem because of the formation of metal droplets from the electrode and their transfer to the weld pool; as a consequence, the interactions are not fully understood.

Recently, Tashiro et al. investigated the full set of processes, from evaporation of metal vapor to fume formation from the metal vapor to predict size and shape of fume particles, by employing two-dimensional GTA and GMA simulation models coupled to a fume formation model which consisted of a homogeneous nucleation model, a condensation model, and a particle coagulation model [8]. The fume formation processes were modeled along several flow pathlines in one-dimensional approach. This allowed the fume formation process to be visualized, and the mechanisms to be theoretically clarified, through numerical analysis. Subsequently, Tashiro et al. also studied the influence of particle charging on the fume formation process considering non-LTE effects by improving the above model and found that particle charging largely affected particle size especially under the non-LTE conditions [9]. Boselli et al. simulated the fume formation process in pulsed GMA welding taking into account the metal transport and metal vapor formation in a self-consistent approach using the volume of fluid (VOF) method and modeling fume particle production using the method of moments (MoM) for the solution of the aerosol general dynamic equation (GDE) [10]. This study allowed one to investigate the fume formation mechanisms in different phases of the current pulse and to track the mass transport of fumes.

Although pure inert shielding gas was used for simplicity in the above simulation studies, in practice, oxygen or carbon dioxide is often mixed with the shielding gas like metal active gas (MAG) welding or CO₂ arc welding for reducing production cost or stabilizing the arc. The concentration of such additional elements in the gas is considered to significantly affect fume formation processes through not only oxidation of the metal vapor and fume particles but also change in arc characteristics leading to different droplet formation and metal transfer phenomena. Sanibondi [11] and also Hunkwan et al. [12] investigated influence of oxidation reactions of Fe on the fume formation process by coupling a fume formation model with a chemical reaction model. They found that FeO particles were preferentially produced in the mixture including oxygen, and the diameter of particles also significantly changed depending on the concentration of oxygen. However, in their study, a

one-way coupling method was used for simplicity to give information such as the vapor pressure calculated in the arc model to the fume formation model as input values. Therefore, for example, time variation in the arc and also consumption of the metal vapor by the fume formation, which affects the current path in the arc, were not taken into account. According to the above limitation, influence of change in the arc characteristics leading to different droplet formation and metal transfer phenomena by mixing additional elements into the gas on the fume formation process is not yet clarified.

We have developed a two-way coupled model consisting of a fume formation model and a GMA welding model taking into account the metal transfer process similar to Boselli's model [10]. With these, we aim to investigate the influence on the fume formation process of the change in arc characteristics leading to different droplet formation and metal transfer phenomena when replacing Ar shielding gas by CO₂.

2 Simulation model

Figure 1 shows an axially symmetric two-dimensional simulation domain (z, r) with a radius of 15 mm and a height of 15 mm consisting of an arc region and a wire region. In CO₂ arc welding, the droplet formation is known to tend to be axially asymmetric leading to repelled transfer especially in the high current range. However, axially symmetric droplet formation is assumed in the present model for simplicity. Regions for a contact tip, a shielding gas inlet, and a nozzle are defined on the top boundary. The outer diameter of the contact tip and the inner diameter of the shielding gas inlet are 2.4 mm and 14 mm, respectively. On the axis, the wire region with a diameter of 1.2 mm and an initial extension of 10 mm corresponding to an arc length of 5 mm is defined. The side boundary is a pressure outlet. The bottom boundary corresponds to the surface of the base metal. The region inside the base metal is not calculated. Non-uniform mesh is used; the maximum and minimum sizes are 0.2 mm and 0.05 mm, respectively. The wire feed speed is 5 m/min. The shielding gas is introduced from the top boundary at a flow rate of 10 L/min. A direct current of 280 A is given at the top boundary. The bottom boundary is set to be 0 V.

Table 1 summarizes simulation conditions. The fume formation processes in argon and CO₂ shielding gases are investigated. In order to strictly model CO₂ arc welding, it is necessary to consider the chemical reaction in the gas and on the droplet surface. As a result of this chemical reaction, the surface tension of the droplet, gas species evaporated from the droplet, and gas species forming fume are also considered to be affected. However, this chemical reaction process is known to be very complicated and has not yet been fully elucidated, so modeling considering all the above factors is difficult at this time. Therefore, in the present study, the model is greatly

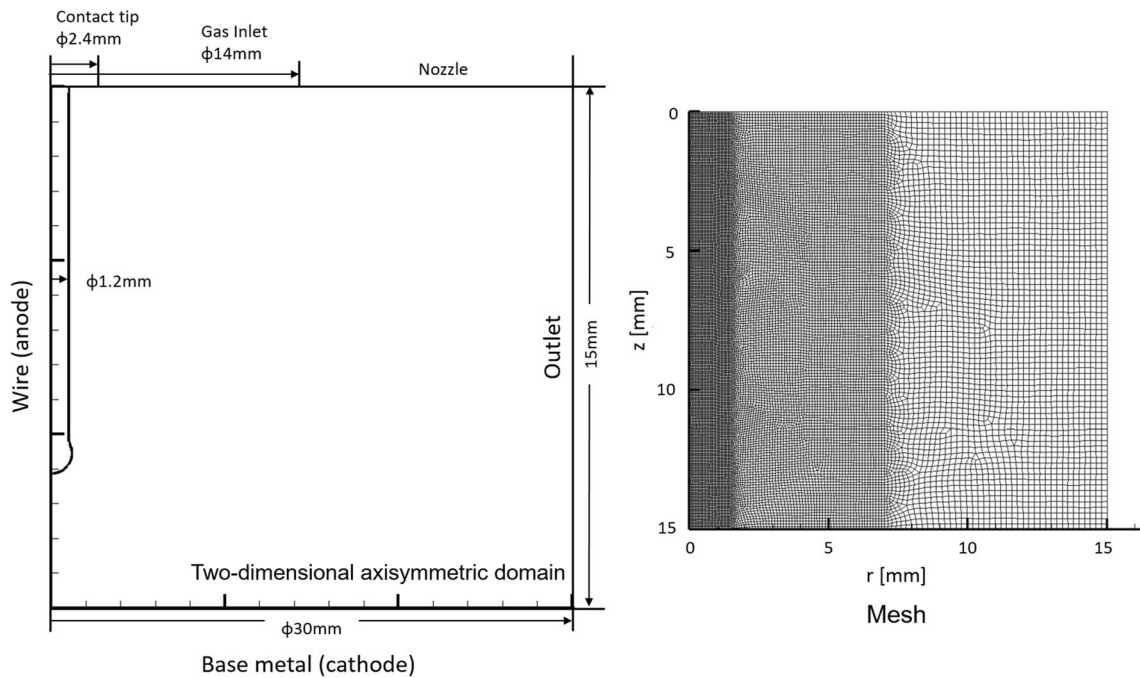


Fig. 1 Schematic diagram of simulation domain

simplified and the investigation is carried out as a virtual experiment ignoring the complicated chemical reaction process and simply taking into account difference in thermodynamic and transport properties between two kinds of gases. In CO₂ arc welding, the gas species evaporated from the molten metal surface are considered to consist mainly of a large amount of Fe and a small amount of FeO, in ratios depending on the surface condition. Thereafter, a part of the Fe is thought to become FeO through the chemical reaction in the gas. Finally, both of Fe and FeO are expected to contribute to the fume formation. In this model, Fe or FeO is assumed to be a gas specie evaporated from the molten metal surface as both extreme cases. The evaporation flux is calculated according to Hertz–Knudsen–Langmuir equation. Similarly, a gas species forming fume through the nucleation and the condensation is also assumed to be Fe or FeO as both extreme cases. In

condition 3, Fe evaporated from the molten metal surface is assumed to be oxidized in the arc to form FeO.

Distributions of flow velocity, temperature, metal vapor concentration, and current density are obtained by solving time-dependent conservation equations of mass, momentum, energy, mass of metal vapor, and current expressed as follows. The magnetic field is obtained from calculation of vector potential. The plasma is assumed to satisfy the LTE condition. The thermodynamic and transport properties of the arc under the LTE condition are calculated as functions of temperature and metal vapor concentration [13]. For simplicity, only Fe is assumed as the metal vapor composition to calculate the above properties, even when FeO is evaporated from the metal surface, for simplicity. The surface tension coefficient of the molten metal of the wire is set to be 1.2 N/m without depending on the shielding gas composition. This assumption is considered to be inevitable for the present calculation which does not take into account the surface oxidation process, because the direction and magnitude of the Marangoni force change in a complicated manner depending on the degree of surface oxidation. The thermodynamic and transport properties of mild steel are used for the wire [14, 15]. VOF method is used for tracking the free surface. The thermodynamic and transport properties at the droplet-plasma boundary are obtained by weighting based on the volume fraction of the metal phase. ANSYS Fluent 18.1 is used for the calculation.

Mass conservation:

$$\frac{\partial \rho}{\partial t} + \nabla \cdot (\rho \vec{u}) = 0 \tag{1}$$

Table 1 Simulation conditions

	Conditions			
	1	2	3	4
Wire composition	Fe			
Wire dimeter (mm)	1.2			
Wire feed speed (min)	5			
Current (A)	DC280			
Gas flow rate (L/min)	10			
Shielding gas	Ar	CO ₂		
Gas species evaporated from molten metal	Fe	Fe	Fe	FeO
Gas species forming fume	Fe	Fe	FeO	FeO

Momentum conservation:

$$\frac{\partial \rho \vec{u}}{\partial t} + \nabla \cdot (\rho \vec{u} \vec{u}) = -\nabla p + \nabla \cdot \vec{\tau} + \rho \vec{g} + \vec{j} \times \vec{B} + \vec{F}_s + \vec{F}_{slid} \quad (2)$$

Energy conservation:

$$\frac{\partial \rho h}{\partial t} + \nabla \cdot (\rho h \vec{u}) = \nabla \cdot (k \nabla T) + \vec{j} \cdot \vec{E} - Q_r + Q_s \quad (3)$$

Mass conservation of metal vapor:

$$\frac{\partial \rho Y}{\partial t} + \nabla \cdot (\rho Y \vec{u}) = \nabla \cdot (\rho D \nabla Y) + M_{\text{evapmetal}} + M_{\text{evapfume}} + M_{\text{fume}} \quad (4)$$

Current conservation:

$$\nabla \cdot \sigma \nabla \Phi = 0 \quad (5)$$

Ohm's law:

$$\vec{j} = -\sigma \nabla \Phi = \sigma \vec{E} \quad (6)$$

Vector potential:

$$\nabla^2 \vec{A} = -\mu_0 \vec{j} \quad (7)$$

Magnetic field:

$$\vec{B} = \nabla \times \vec{A} \quad (8)$$

where ρ is the mass density, \vec{u} is the velocity, p is the pressure, $\vec{\tau}$ is the viscous stress tensor, \vec{g} is the gravity, \vec{j} is the current density, \vec{B} is the magnetic field, \vec{F}_s is a source term for surface tension force, \vec{F}_{slid} is a source term to express the behavior of the solid region, h is the enthalpy, k is the thermal conductivity, T is the temperature, \vec{E} is the electric field, Q_r is a source term for arc radiation, Q_s is a source term for electron condensation, surface radiation, and latent heat of vaporization on the wire surface, Y is the mass fraction of metal vapor, D is the diffusion coefficient of metal vapor, $M_{\text{evapmetal}}$ is a source term for evaporation of metal calculated simply by Hertz–Knudsen–Langmuir equation, M_{evapfume} is a source term for evaporation of fume, M_{fume} is a source term for nucleation and condensation, Φ is the electric potential, and \vec{A} is the vector potential.

Figure 2 shows saturation vapor pressure used for calculating Hertz–Knudsen–Langmuir equation. The saturation vapor pressure of FeO is seen to be approximately 10 times larger than that of Fe to lead to larger evaporation rate.

Table 2 summarizes boundary conditions, where u_{wire} and u_{gas} are velocities corresponding to the wire feed speed and the

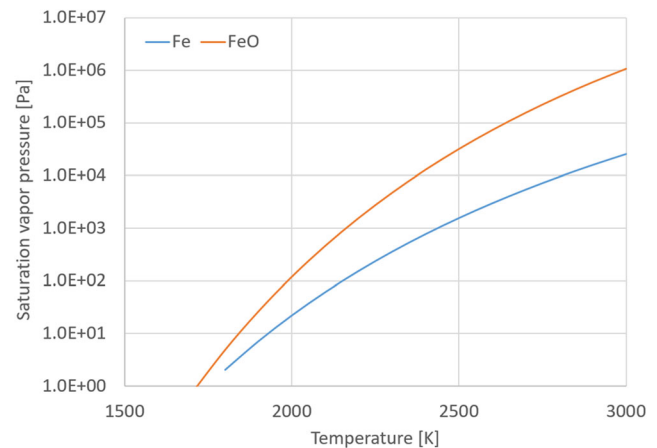


Fig. 2 Comparison of saturation vapor pressure between Fe and FeO

shielding gas flow rate. In order to consider evaporation of the metal vapor also from the weld pool surface, the temperature on the base metal is assumed to be 1800 K for $r < 5$ mm and 300 K for $r > 5$ mm [16]. P_{atm} is an atmospheric pressure. j_{given} is the current density corresponding the input current.

The fume formation model considers the homogeneous nucleation, the heterogeneous condensation, and the coagulation. In this study, MoM equations expressed as follows are employed for reducing calculation cost. In this model, it is assumed that the fume is spherical, the temperature of the fume is the same as the plasma, and the fume size follows unimodal lognormal distribution. The detail of this model is described in the literatures [10, 17–19].

$$M_k = \int_0^\infty v_p^k n(v_p) dv_p \quad (9)$$

$$\frac{\partial M_k}{\partial t} + \nabla \cdot (M_k \vec{u}) = \nabla \cdot (D_k \nabla M_k) + [M_k]_{\text{nucl}} + [M_k]_{\text{cond}} + [M_k]_{\text{coag}} - [M_k]_{\text{evap}} \quad (10)$$

$$(k = 0, 1, 2)$$

$$\ln^2 \sigma_g = \frac{1}{9} \ln \left(\frac{M_0 M_2}{M_1^2} \right) \quad (11)$$

$$v_g = \frac{M_1^2}{M_0^{3/2} M_2^{1/2}} \quad (12)$$

$$M_k = M_0 v_g^k \exp(4.5 k^2 \ln^2 \sigma_g) \quad (13)$$

where M_k is the k th moment, v_p is the particle volume, n is the particle size distribution function, D_k is the diffusion coefficient for k th moment [19], $[M_k]$ is the net production rates due to nucleation, condensation, coagulation, and evaporation, σ_g is the geometric standard deviation, and v_g is the geometric mean volume. The fume formation rate (metal vapor consumption rate), the fume mass density (product of the first

Table 2 Boundary conditions

Boundary	Mass and momentum	Mass fraction of metal vapor	Energy	Electric potential	Magnetic potential
Wire inlet	$\vec{u} = \vec{u}_{\text{wire}}$	$\partial Y/\partial n = 0$	300 K	$-\sigma \partial \Phi/\partial n = j_{\text{given}}$	$\partial Ai/\partial n = 0$
Contact tip	$\vec{u} = 0$	$\partial Y/\partial n = 0$	300 K	$\partial \Phi/\partial n = 0$	$\partial Ai/\partial n = 0$
Gas inlet	$\vec{u} = \vec{u}_{\text{gas}}$	$y = 0$	300 K	$\partial \Phi/\partial n = 0$	$\partial Ai/\partial n = 0$
Nozzle	$\vec{u} = 0$	$\partial Y/\partial n = 0$	300 K	$\partial \Phi/\partial n = 0$	$\partial Ai/\partial n = 0$
Gas outlet	$P = P_{\text{atm}}$	$y = 0$	300 K	$\partial \Phi/\partial n = 0$	$Ai = 0$
Base metal	$\vec{u} = 0$	$\partial Y/\partial n = 0$	1800 K ($r \leq 5$ mm) 300 K ($r > 5$ mm)	$\Phi = 0$	$\partial Ai/\partial n = 0$
Axis	$\partial u/\partial n = 0$	$\partial Y/\partial n = 0$	$\partial T/\partial n = 0$	$\partial \Phi/\partial n = 0$	$\partial Ai/\partial n = 0$

moment and mass density of metal), and fume diameter (volume mean diameter) are calculated.

3 Results and discussion

Firstly, the fume formation process in Ar GMA welding is discussed. The calculated arc voltages in Ar GMA welding were approximately 25 V. Figures 3, 4, 5, and 6 show distributions of temperature, mole fraction of metal vapor, fume formation rate, and fume mass density at five moments ($t = 0, 4, 6, 8,$ and 10 ms) in condition 1. The arc temperature in the Ar plasma reached approximately 12,000 K at the maximum. Conversely, the arc temperature in dense metal vapor plasma around the axis decreased to around 7000 K. Both

temperatures agree well with the result of the spectroscopic measurement [20]. The droplet temperature was raised to approximately 2500 K on average and maximally 2800 K on the surface due to the heating by the electron condensation and the thermal conduction from the arc plasma. Consequently, large amount of metal vapor was evaporated from the droplet surface, and most of the metal vapor was transported to the base metal by the plasma jet. Afterward, the metal vapor transported radially outward to the low temperature arc plasma around 2000 K in the downstream region of the plasma jet produced fume through the nucleation. Then, the fume, which grew due to the condensation and coagulation, was transported to the surrounding by convection and diffusion. The droplet was detached from the wire tip immediately after $t = 4$ ms and then transferred to the base metal. It was seen that

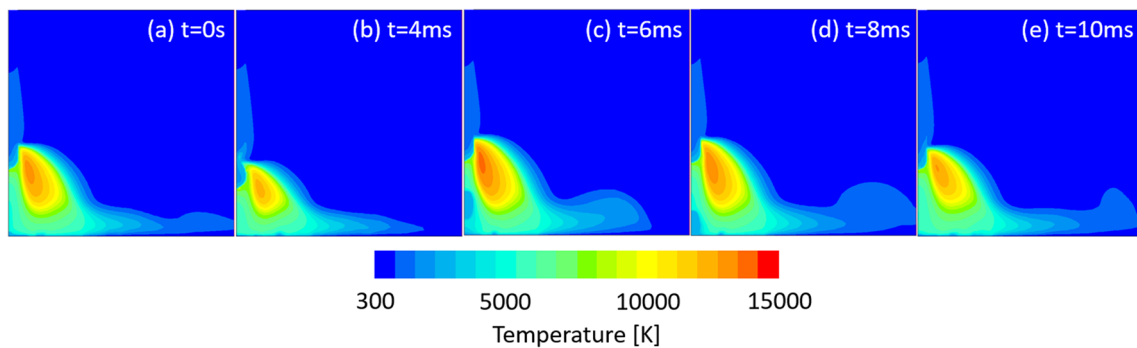


Fig. 3 Distributions of temperature in condition 1

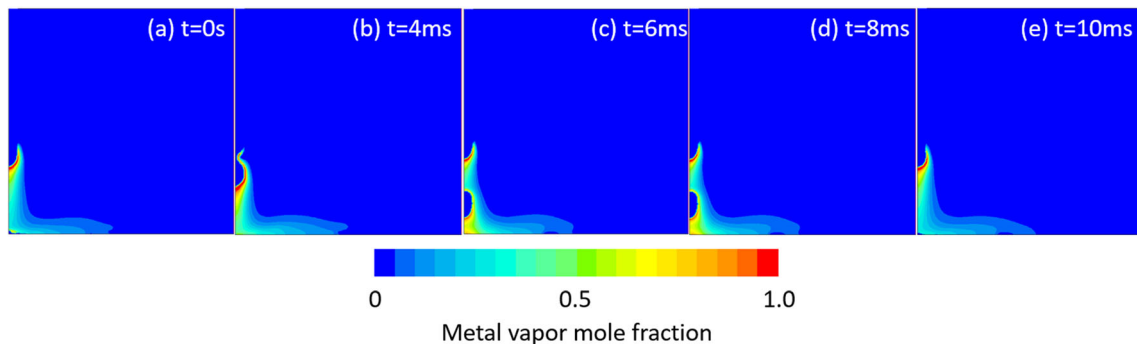


Fig. 4 Distributions of mole fraction of metal vapor in condition 1

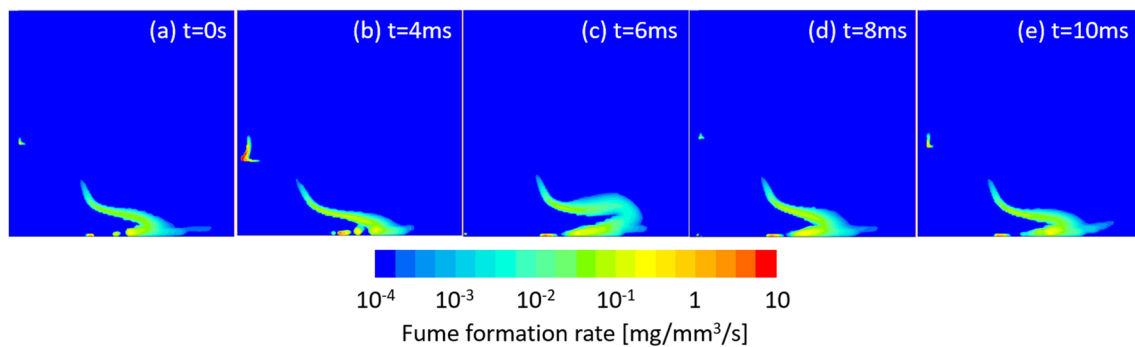


Fig. 5 Distributions of fume formation rate in condition 1

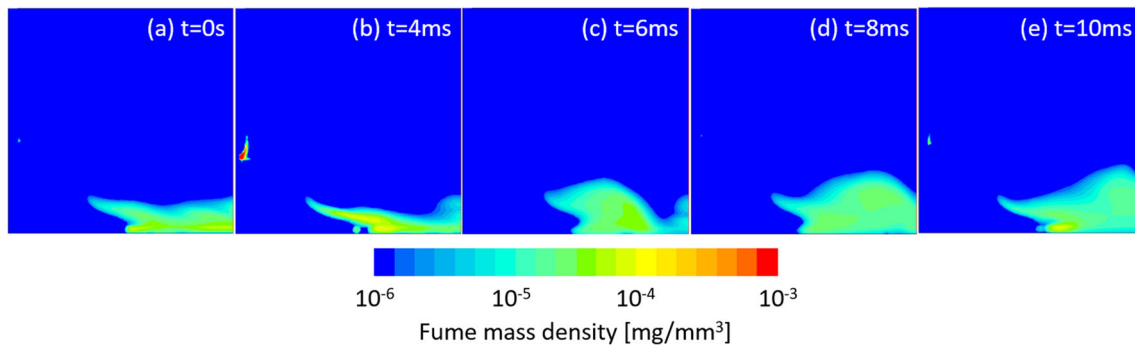


Fig. 6 Distributions of fume mass density in condition 1

a very thin neck was formed between the droplet and the wire around $t = 4$ ms and the fume formation rate highly increased around the neck. As a result, it was clarified that the fume was formed also in the upstream region of the plasma jet near the droplet as well as in the downstream region near the base metal. However, most of the former was transported into the arc and evaporated and returned to the metal vapor again.

Secondly, the fume formation process in CO_2 arc welding is discussed. The calculated arc voltages in CO_2 arc welding were approximately 35 V. Figures 7, 8, 9, and 10 show distributions of temperature, mole fraction of metal vapor, fume formation rate, and fume mass density at five moments ($t = 0, 4, 6, 8,$ and 10 ms) in condition 4. It is well-known that the arc is strongly constricted under the droplet due to large

specific heat in CO_2 arc welding [21]. The size of the droplet became significantly larger than that of Ar GMA welding, because the droplet was lifted up due to the higher arc pressure caused by the constriction of the arc. Although metal vapor was evaporated from the entire surface of the droplet, metal vapor outside the arc root was consumed immediately after evaporation to produce a large amount of the fume due to rapid cooling by the surrounding low temperature gas. A part of the fume around the droplet was directly transported to the surrounding without being evaporated again in the arc.

Figure 11 shows a comparison of distributions of fume diameter in condition 1~4 at $t = 10$ ms. Table 3 shows summary of the simulation results at $t = 10$ ms. Although this investigation was carried out as a virtual experiment under

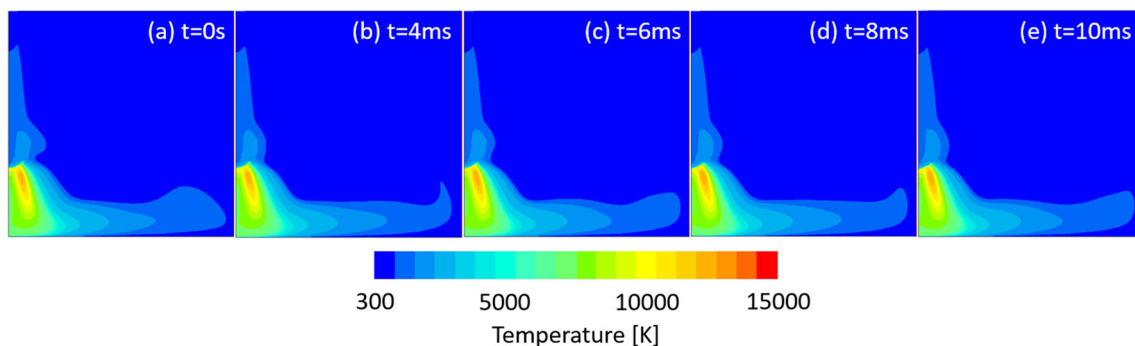


Fig. 7 Distributions of temperature in condition 4

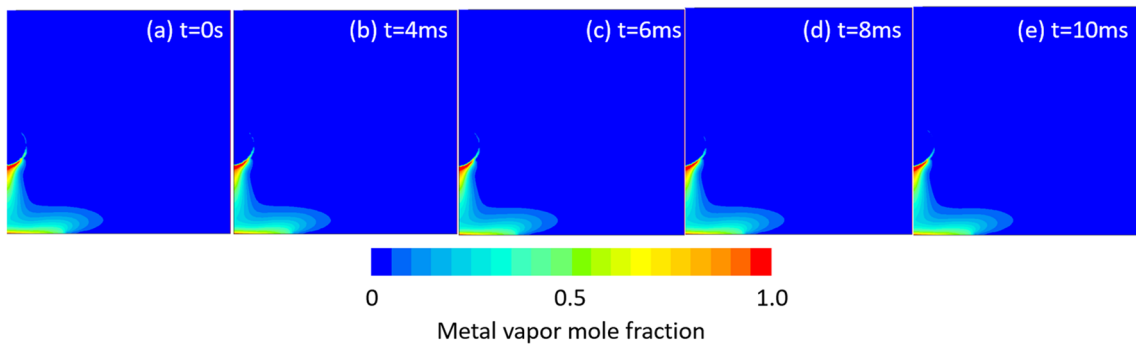


Fig. 8 Distributions of mole fraction of metal vapor in condition 4

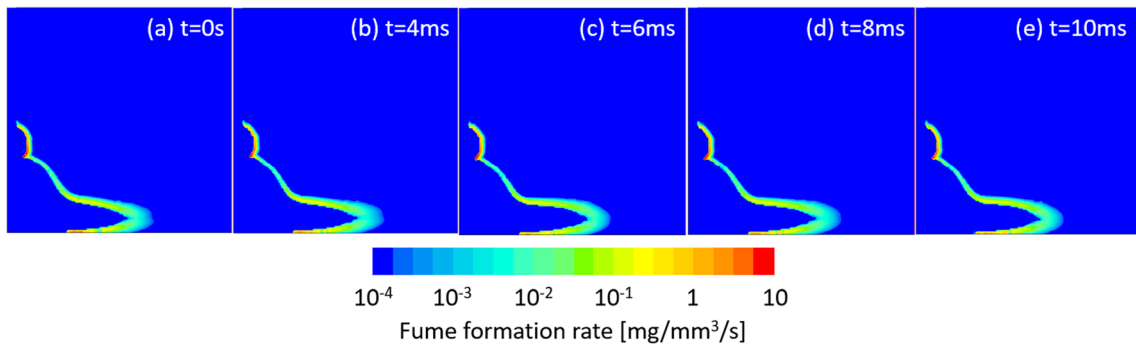


Fig. 9 Distributions of fume formation rate in condition 4

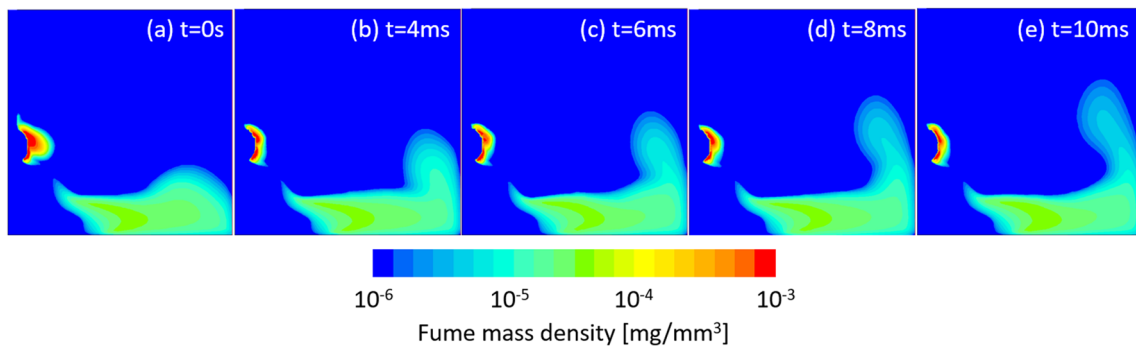


Fig. 10 Distributions of fume mass density in condition 4

Fig. 11 Distributions of fume diameter

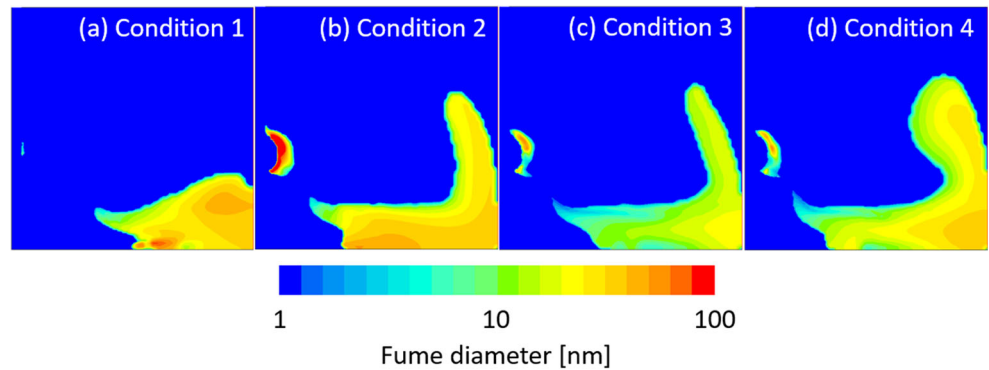
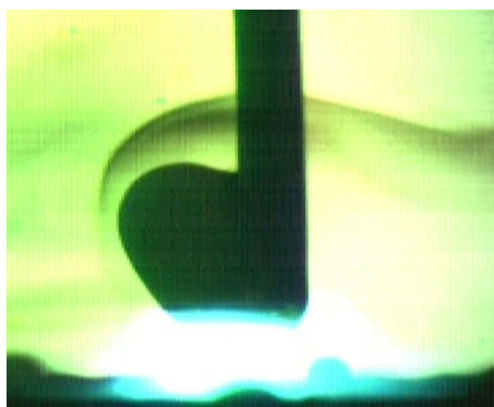


Table 3 Summary of simulation results

	Conditions			
	1	2	3	4
Shielding gas	Ar	CO ₂		
Gas species evaporated from droplet	Fe	Fe	Fe	FeO
Gas species forming fume	Fe	Fe	FeO	FeO
Fume formation rate (FFR) (mg/s)	13.1	12.5	12.4	23.2
Ratio of fume transported directly from droplet to surrounding (%)	–	29.7	25.4	26.5
Fume diameter (near droplet) (nm)	–	160.2	45.4	48.8
Fume diameter (downstream) (nm)	45.5	39.5	18.3	28.5

the strong assumptions, a quantitative comparison for each condition taking into account its variation range is thought to be valid, because this range roughly covers possible lowest and highest values. In Ar GMA welding, the fume produced around the neck immediately before the detachment of the droplet was evaporated again in the arc. Then, this vapor was transported to the downstream region of the plasma jet and produced fume with an averaged size of 45.5 nm there. In CO₂ arc welding, the diameter of the fume produced around the droplet exceeded 100 nm maximally because of the large quenching rate of the arc. In contrast, the size of the fume produced in the downstream region of the plasma jet was only approximately 20–40 nm on average. When FeO was assumed as a gas species forming the fume, the fume diameter became smaller than that of Fe, because the number of particles produced by the nucleation increased mainly due to a lower surface tension. When FeO was assumed as gas species evaporated from molten metal, the fume formation rate and the diameter of the fume increased because of an increase in the evaporation rate. Furthermore, approximately 30% of all fume particles produced around the droplet were transported directly to the surroundings, and the other particles were transported into the arc to be evaporated to produce fume particles in the downstream region in CO₂ arc welding. This tendency agreed well with appearance of the fume observed in the experiment shown in Fig. 12.

**Fig. 12** Appearance of fume in CO₂ arc welding

The total fume formation rate integrated in the entire region was around 10–20 mg/s, which was slightly larger than experimental results: for example, maximally 2.8 mg/s in Ar + 2%CO₂ measured by Pires et al. [22] or 13.3 mg/s in Ar + 38%He+2%CO₂ measured by Ioffe et al. [23]. This overestimation is considered to be mainly caused by the excessive arc current against the wire feed speed compared to that of an actual welding condition. However, the discussions in the above comparative study are thought to be still valid, although these points should be modified in future for improving the accuracy of the model. The degree of the oxidation on the droplet surface was suggested to be linked to the fume formation rate in CO₂ arc welding. Considering the above, further studies are planned to investigate the influence of the degree of oxidation on the droplet surface on the fume formation process as well as the fume formation rate taking the oxidation process on the droplet surface into account in the model. Furthermore, it is also necessary to be investigated the influence of the occurrence of short circuiting transfer on the fume formation process in the case of CO₂ arc welding.

4 Conclusions

A fume formation model consisting of a homogeneous nucleation model, a heterogeneous condensation model, and a coagulation model was coupled with a GMA welding model. This model allowed us to investigate a series of processes such as evaporation of metal vapor from the molten metal, transport of the metal vapor in the arc, fume formation from the metal vapor, and transport of the fume to the surroundings. The influence on the fume formation process of the change in arc characteristics leading to different droplet formation and metal transfer phenomena when replacing Ar shielding gas by CO₂ was investigated using this model. As a result, it was clarified that the fume particles produced around the droplet were transported into the arc to be evaporated again and a large number of fine fume particles were produced in the downstream region of the plasma flow near the base metal in Ar GMA welding. In contrast, approximately 30% of all fume

particles produced around the droplet were transported directly to the surrounding, and the other particles were transported into the arc to be evaporated to produce fume particles in the downstream region in CO₂ arc welding.

Funding This work was supported by JSPS KAKENHI Grant Number JP25420779.

References

1. Terasaki H, Tanaka M, Ushio M (2002) Effects of metal vapor on electron temperature in helium gas tungsten arcs. *Metall Mater Trans A* 33:1183–1188
2. Murphy AB (2010) The effects of metal vapour in arc welding. *J Phys D Appl Phys* 43:434001
3. Antonini JM (2003) Health effects of welding. *Crit Rev Toxicol* 33: 61–103
4. Kobayashi M, Maki S, Hashimoto Y, Suga T (1980) Investigations on fume generating phenomena of shielded metal arc welding. *J Japan Weld Soc* 49:454–461
5. Jenkins NT, Eagar TW (2005) Chemical analysis of welding fume particles. *Weld J* 84:87s–93s
6. Bosworth MR, Deam RT (2000) Influence of GMAW droplet size on fume formation rate. *J Phys D Appl Phys* 33:2605–2610
7. Deam RT, Simpson SW, Haidar J (2000) A semi-empirical model of the fume formation from gas metal arc welding. *J Phys D Appl Phys* 33:1393–1402
8. Tashiro S, Zeniya T, Yamamoto K, Tanaka M, Nakata K, Murphy AB, Yamamoto E, Yamazaki K, Suzuki K (2010) Numerical analysis of fume formation mechanism in arc welding. *J Phys D Appl Phys* 43:434012
9. Tashiro S, Murphy AB, Matsui S, Tanaka M (2013) Numerical analysis of the influence of particle charging on the fume formation process in arc welding. *J Phys D Appl Phys* 46:224007
10. Boselli M, Colombo V, Ghedini E, Gherardi M, Sanibondi P (2013) Two-dimensional time-dependent modelling of fume formation in a pulsed gas metal arc welding process. *J Phys D Appl Phys* 46: 224006
11. Sanibondi P (2015) Numerical investigation of the effects of iron oxidation reactions on the fume formation mechanism in arc welding. *J Phys D Appl Phys* 48:345202
12. Park H, Mudra M, Trautmann M, Murphy AB (2017) A coupled chemical kinetic and nucleation model of fume formation in metal-inert-gas/metal-active-gas welding. *Plasma Chem Plasma Process* 37:805–823
13. Tanaka M, Yamamoto K, Tashiro S, Nakata K, Yamamoto E, Yamazaki K, Suzuki K, Murphy AB, Lowke JJ (2010) Time-dependent calculations of molten pool formation and thermal plasma with metal vapour in gas tungsten arc welding. *J Phys D Appl Phys* 43:434009
14. Hertel M, Spille-Kohoff A, Fussel U, Schnick M (2013) Numerical simulation of droplet detachment in pulsed gas–metal arc welding including the influence of metal vapour. *J Phys D Appl Phys* 46: 224003
15. Ogino Y, Hirata Y, Murphy AB (2016) Numerical simulation of GMAW process using Ar and an Ar–CO₂ gas mixture. *Weld World* 60:345–353
16. Yamazaki K, Yamamoto E, Suzuki S, Koshiishi F, Miyazako S, Tashiro S, Tanaka M, Nakata K (2009) The surface temperature measurement of weld pool by infrared two-color pyrometry. *Quarterly J Japan Welding Soc* 27:34–40
17. Pratsinis SE (1988) Simultaneous nucleation, condensation, and coagulation in aerosol reactors. *J Colloid Interface Sci* 124:416–427
18. Phanse GM, Pratsinis SE (1989) Theory for Aerosol Generation in Laminar Flow Condensers. *Aerosol Sci Technol* 11:100–119
19. Aristizabal F, Munz RJ, Berk D (2006) Modeling of the production of ultra fine Aluminium particles in rapid quenching turbulent flow. *Aerosol Sci* 37:162–186
20. Tsujimura Y, Tanaka M (2012) Analysis of behaviour of arc plasma conditions in MIG welding with metal transfer - Visualization of Phenomena of Welding Arc by Imaging Spectroscopy Quarterly. *J Japan Welding Soc* 30:288–297
21. Tanaka M, Tashiro S, Satoh T, Murphy AB, Lowke JJ (2008) Influence of shielding gas composition on arc properties in TIG welding. *Sci Technol Weld Join* 13:225–231
22. Pires I, Quintino L, Miranda RM (2007) Analysis of the influence of shielding gas mixtures on the gas metal arc welding metal transfer modes and fume formation rate. *Mater Des* 28:1623–1631
23. Ioffe I, MacLean D, Perelman N, Stares I, Thornton M (1995) Fume formation rate at globular to spray mode transition during welding. *J Phys D Appl Phys* 28:2473–2477